Aalborg Universitet

AALBORG UNIVERSITY
DENMARK

Robust DOA Estimation in Satellite Systems in Presence of Coherent Signals Subject to Low SNR

Li, Yunfeng; Huang, Yonghui; Ren, Jian; Liu, Ying; Pedersen, Gert Frolund; Shen, Ming

Published in:
IEEE Access

DOI (link to publication from Publisher):
10.1109/ACCESS.2022.3213712

Creative Commons License
CC BY-NC-ND 4.0

Publication date:
2022

Document Version
Publisher's PDF, also known as Version of record

Link to publication from Aalborg University

Citation for published version (APA):
Li, Y., Huang, Y., Ren, J., Liu, Y., Pedersen, G. F., & Shen, M. (2022). Robust DOA Estimation in Satellite Systems in Presence of Coherent Signals Subject to Low SNR. *IEEE Access*, *10*, 109983-109993. https://doi.org/10.1109/ACCESS.2022.3213712

General rights
Copyright and moral rights for the publications made accessible in the public portal are retained by the authors and/or other copyright owners and it is a condition of accessing publications that users recognise and abide by the legal requirements associated with these rights.

- Users may download and print one copy of any publication from the public portal for the purpose of private study or research.
- You may not further distribute the material or use it for any profit-making activity or commercial gain
- You may freely distribute the URL identifying the publication in the public portal -

Take down policy
If you believe that this document breaches copyright please contact us at vbn@aub.aau.dk providing details, and we will remove access to the work immediately and investigate your claim.

IEEE Access
Multidisciplinary | Rapid Review | Open Access Journal

Received 13 September 2022, accepted 4 October 2022, date of publication 10 October 2022, date of current version 20 October 2022.

Digital Object Identifier 10.1109/ACCESS.2022.3213712

RESEARCH ARTICLE

Robust DOA Estimation in Satellite Systems in Presence of Coherent Signals Subject to Low SNR

YUNFENG LI[1,2], (Student Member, IEEE), YONGHUI HUANG[1], JIAN REN[3], (Member, IEEE), YING LIU[4], GERT FRØLUND PEDERSEN[5], (Senior Member, IEEE), AND MING SHEN[5], (Senior Member, IEEE)

[1]National Space Science Center, Chinese Academy of Sciences, Beijing 100190, China
[2]School of Electronic, Electrical and Communication Engineering, University of Chinese Academy of Sciences, Beijing 100049, China
[3]National Key Laboratory of Antennas and Microwave Technology, Xidian University, Shaanxi 710071, China
[4]School of Electronic and Information Engineering, Beijing Jiaotong University, Beijing 100044, China
[5]Department of Electronic Systems, Aalborg University, 9220 Aalborg, Denmark

Corresponding author: Yonghui Huang (yonghui@nssc.ac.cn)

This work was supported by the China Scholarship Council under Grant 202004910734.

ABSTRACT Signal source number detection is an essential issue for the direction of arrival (DOA) estimation in satellite communication systems. The performances of conventional and deep-learning-based signal source number detection methods will deteriorate when the signal-to-noise ratio is low or coherent signals exist. This paper proposes a DOA detection network (DTN) combined with the root weighted subspace fitting (root-WSF) method to tackle this challenge. The DTN uses the constructed deep neural networks (DNN) to denoise the received signals and captures the nonlinear mapping relationship between the received signals and the number of signal sources. The received signals in the complex-valued domain are directly treated as DTN's input, and the label of DTN is the one-hot encoding of the source number. It solves the issue that the classifier cannot well-handle the coherent signals and extends the values of discrete features to Euclidean space. Accordingly, the trained DTN can detect the signal source numbers with an average detection accuracy of 96.6%, and the root-WSF algorithm is applied as the rear stage of DOA estimation. Compared with the traditional DOA methods, the proposed DTN incorporated with the root-WSF algorithm features superior robustness, high DOA estimation accuracy, and enhanced resolution.

INDEX TERMS Deep neural network (DNN), direction of arrival (DOA), DOA detection network (DTN), root weighted subspace fitting (root-WSF), satellite communication system.

I. INTRODUCTION

With the development of satellite communication systems, radio spectrum resources have become scarce [1]. This causes interference on the earth's surface as well as in space, which poses massive threats to regular satellite communications [2], [3]. Hence, the array signal processing has received even more attention in recent years, and the direction of arrival (DOA) is one of the essential topics in the field of array signal processing. Multiple super-resolution DOA estimation methods have been discussed, such as the maximum likelihood (ML) [4], multiple signal classification (MUSIC) [5], estimation of signal parameters via rotational invariance techniques (ESPRIT) [6], weighted subspace fitting (WSF) [7], as well as other performance improved algorithms [8], [9]. They provide bases for anti-interference technologies by accurately estimating the real-time DOA of the interference signal. Nevertheless, most super-resolution DOA estimation methods require prior knowledge regarding the number of signal sources. Unfortunately, it is not straightforward to guarantee this assumption in practice [10]. Therefore, the detection of signal source numbers is an essential issue for DOA estimation.

Many scholars have proposed effective methods for detecting the number of signal sources. The most widely used ones are the Akaike information theory (AIC) and minimum

The associate editor coordinating the review of this manuscript and approving it for publication was Pasquale De Meo.

This work is licensed under a Creative Commons Attribution-NonCommercial-NoDerivatives 4.0 License.
For more information, see https://creativecommons.org/licenses/by-nc-nd/4.0/

TABLE 1. Investigation of previous studies on DOA estimation problems based on neural networks.

Method	Receive antenna	Signal type	Spatial scope	SNR	Source number	Angle separation
RNEAT [15]	URA (8)	Uncorrelated	$[0°, 360°]$	$[-10$ dB, 10 dB$]$	Random	Random
CNN [17]	UCA (8)	Uncorrelated	$[0°, 360°]$	[0 dB, 5 dB]	Fixed	$1°$
LCN-CNN [18]	–	Echo signals	$[-80°, +80°]$	$[-10$ dB, 10 dB$]$	Fixed	$20°$
DNN-based DOA [19]	ULA (1*10)	Uncorrelated	$[-60°, +60°)$	10 dB	Fixed	$1°$
DNN-DOA [20]	ULA (1*10)	Uncorrelated	$[-60°, +60°]$	$[-10$ dB, 10 dB$]$	Fixed	$2°$ and $7.5°$
CNN [21]	ULA (1*8)	Non-Coherent	$[45°, 60°, 75°]$	$[-20$ dB, 20 dB$]$	Fixed	$15°$
ERNet & ECNet [22]	ULA (1*10)	Coherent & non-Coherent	$[0°, 180°]$	[0 dB, 40 dB]	Random	Random
BPNN [23]	ULA (1*8)	Coherent	$[0°, 180°]$	$[-20$ dB, 20 dB$]$	Fixed	$20°$
DTN (Proposed)	**ULA (1*10)**	**Coherent & non-Coherent**	$[-90°, 90°]$	**$[-20$ dB, 20 dB$]$**	**Random**	**Random**

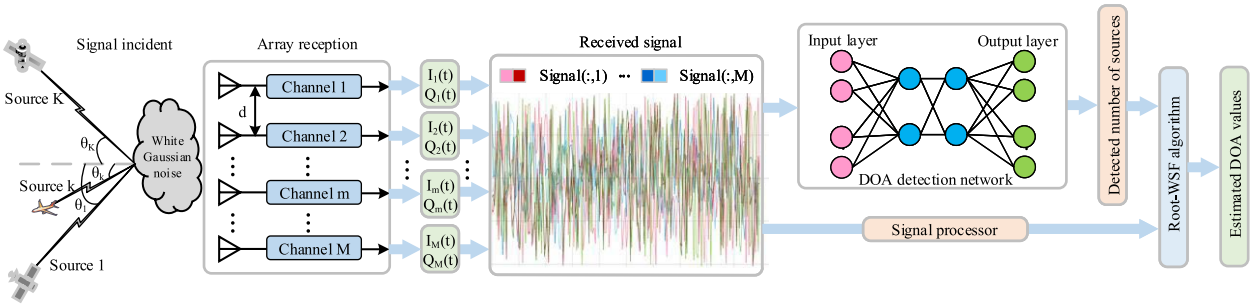

FIGURE 1. DOA estimation system model of antenna array in receiver system, in which the DOA detection network (DTN) incorporated with root-WSF algorithm to estimate DOA values.

description length (MDL) criterion. As stated in [11], the AIC criterion is not a consistent estimation. Even in the case of a high number of snapshots, it still has a relatively significant error probability. Conversely, the MDL criterion is a consistent estimation with superior performance under a high signal-to-noise ratio (SNR). However, it performs unsatisfactorily in low SNR scenarios compared with AIC [11]. Besides, both methods are highly sensitive to the received signals and their noise models. The signal source number cannot be estimated correctly when coherent signals exist in signal sources.

However, coherent signal sources are ubiquitous in practice, such as multi-path signal transmission or electromagnetic interference intentionally released by the adversary [10]. In the case scenario where the signal sources are coherent, some coherent sources' steering vector is not entirely orthogonal to the noise subspace. Subsequently, the DOA cannot be correctly estimated by conventional methods, e.g., MUSIC [5], etc., even if the signal source number is known. Two types of approaches are proposed to handle this issue: spatial smoothing based on dimensionality reduction [12] and WSF without pre-processing [13]. However, the spatial smoothing operation reduces the array's effective aperture [12], and the DOA estimation variance will increase as the sub-array is smaller than the original array. The WSF exhibits a more accurate performance to estimate the coherent signal sources. However, it is still mandatory for WSF to correctly detect the signal source number as a premise. Otherwise, the performance of WSF will be significantly deteriorated [13].

In recent years, deep learning has been widely used in various fields due to its enhanced ability to solve complicated nonlinear problems [14], [15], [16]. It also provides an advanced solution for conventional DOA estimation. Several works studying the neural-network-based DOA estimation [17], [18], [19], [20] are on the premise of fixed target source numbers, as summarized in Table 1. Compared with the traditional MUSIC and ESPRIT methods, they lessen the required computational complexity and accomplish a greater DOA estimation accuracy. However, these studies are limited to the scenarios with the prior-known signal source number [17], [18], [19], [20], the larger angular differences among signal sources [18], or the same SNR [19]. In practice, the number of signal sources is unknown, and the priority of DOA estimation is to detect the number of signal sources accurately. Recently, deep-learning-based methods for detecting signal source numbers can be found in [21], [22], and [23], as summarized in Table 1. Compared with the traditional AIC and MDL methods, the convolutional neural network (CNN) [21] successfully demonstrates its application prospects. Nonetheless, it is only effective when the signal sources are independent. In [22], the authors propose a deep neural network (DNN)-based eigenvalue classification network (ECNet), which can handle coherent sources by adopting the forward-backward spatial smoothing technique. The eigenvalues covariance matrix is adopted as inputs, which is identical to AIC and MDL approaches. Moreover, the authors in [23] estimate the number of coherent signals based on the spatial difference smoothing of the array data. However, by using spatial smoothing, the effective array apertures are decreased in [22] and [23]. Consequently, the sub-array is smaller than the original array, and the variance of the estimator increases.

This paper proposes an improved method for the accurate detection of signal source numbers based on the constructed DOA detection network (DTN). Besides, the robust

root-WSF is incorporated with DTN to estimate DOA angles. The contributions of this paper are listed as follows:

- A well-trained DTN is used to estimate the signal source number accurately. The received signals in the complex-valued domain are directly adopted as input, and the informative features are denoised and non-linearly transformed. The label of DTN is the one-hot encoding of the source number, which solves the problem that the classifier cannot handle the coherent signals and extends the values of discrete features to Euclidean space.
- The performances of the conventional AIC and MDL, the neural-networks-based CNN and ECNet, and the proposed DTN method are compared. Simulation results show that this method can effectively detect the numbers of both non-coherent and coherent signal sources with high robustness, even under a low SNR scenario.
- On the basis of the proposed DTN, the root-WSF algorithm is incorporated to handle the issue that the array aperture is to be sacrificed to improve the estimation accuracy and resolution.
- Validations are performed to evaluate the method's scalability under sufficient condition variations, including the number of target sources, angle range, SNRs, and snapshots. The results show that the proposed DTN has superior robustness in estimating signal source numbers.

This paper is organized as follows. The received signal model, root-WSF method, and the DTN algorithm are presented in Section II. The detailed simulation results, error analysis, and performance comparisons under different situations are presented in Section III. Section IV compares the DOA estimation performances of ESPRIT, MUSIC, root-MUSIC, and root-WSF, given the correct signal source number provided by the proposed DTN. Finally, Section V concludes this paper.

II. MATHEMATICAL FORMULATION

A. SIGNAL MODEL

As shown in Fig. 1, the DOA estimation system comprises three parts: signal incident, array reception, and parameter estimation [10]. The number of array elements is assumed to be equal to the number of channels. Parameter estimation uses array signal processing technology to extract the spatial incident signal's characteristic parameters from the data received by the antenna array. The received data includes the information on the array signal and the complex spatial environment characteristics. It also includes error information such as mutual coupling, channel inconsistency, frequency band inconsistency, etc. The mathematical model of the signal received by the antenna array will be described in the following subsections.

B. RECEIVED SIGNAL MODEL

It is supposed that K narrow-band signals in the far-field are incident on a uniform linear array (ULA), and the antenna array is composed of M elements. The received data can be expressed in the form of a complex envelope as:

$$s_k(t) = u_k(t)\, e^{j(\omega_0 t + \varphi(t))}, \tag{1}$$

where $u_k(t)$ and $\varphi(t)$ are the amplitude and phase of the received signal, respectively. Besides, $\omega_0 = 2\pi f = 2\pi \frac{c}{\lambda}$ is the frequency of the received signal, where c and λ are the light speed and wavelength, respectively. When considering the delay between elements,

$$s_k(t-\tau) = u_k(t-\tau)\, e^{j(\omega_0(t-\tau)+\varphi(t-\tau))}. \tag{2}$$

Under the scenario with the signal bandwidth $BW \ll f/D$, $s_k(t)$ is a narrow-band signal, and D denote the aperture of the ULA. It exists that

$$\begin{cases} u_k(t-\tau) \approx u_k(t) \\ \varphi(t-\tau) \approx \varphi(t). \end{cases} \tag{3}$$

Hence, Eq. (2) can be re-written as

$$s_k(t-\tau) \approx s_k(t)\, e^{-j\omega_0 \tau}, \tag{4}$$

where $k = 1, 2, \ldots, K$. Then the received signal of the m^{th} array element can be obtained as:

$$x_m(t) = \sum_{k=1}^{K} g_{mk} s_k(t-\tau_{mk}) + n_m(t). \tag{5}$$

In (5), $m = 1, 2, \ldots, M$, and g_{mk} is the gain of the m^{th} element to the k^{th} signal. $n_m(t)$ is the white Gaussian noise of the m^{th} element at the time instant t. Expression τ_{mk} denotes the time delay in relative to the reference element when the k^{th} signal reaches the m^{th} element, which is obtained by

$$\tau_{mk} = \frac{1}{c}(p_m sin\theta_k), \tag{6}$$

where p_m is the array element's position with the origin as the reference point, and θ_k is the azimuth angle of the assumed signal source.

Arranging the signals received by M array elements at time t into a column vector, $\mathbf{X(t)}$ can be given by (7), as shown at the bottom of the next page. Ideally, assuming that the array elements are isotropic and there is no channel inconsistency, mutual coupling, and other factors, the gain in (7) can be assumed to be 1, and (8), as shown at the bottom of the next page, can be obtained.

The vector form of (8) can be expressed as

$$\mathbf{X}(\mathbf{t}) = \mathbf{AS}(\mathbf{t}) + \mathbf{N}(\mathbf{t}), \tag{9}$$

where $A = \left[a_1(\omega_0)\ a_2(\omega_0) \cdots a_K(\omega_0)\right]$ is the steering matrix [10], and its steering vector can be written as

$$a_k(\omega_0) = \begin{bmatrix} e^{(-j\omega_0\tau_{1k})} \\ e^{(-j\omega_0\tau_{2k})} \\ \vdots \\ e^{(-j\omega_0\tau_{Mk})} \end{bmatrix} = \begin{bmatrix} e^{\left(-j\frac{2\pi}{\lambda}p_1 \sin\theta_k\right)} \\ e^{\left(-j\frac{2\pi}{\lambda}p_2 \sin\theta_k\right)} \\ \vdots \\ e^{\left(-j\frac{2\pi}{\lambda}p_M \sin\theta_k\right)}. \end{bmatrix} \tag{10}$$

TABLE 2. Procedure of DTN.

Algorithm: The DOA detection network (DTN)
$Step1$: Generate the set of training data X_{train} and test data X_{test} of DOAs. Calculate the received signal using (9) and (13), and mark the target source number with label Y.
$Step2$: Initialization the DTN model parameters w and b.
$Step3$: Present the training data X_{train} to the detection network and update w and b by SGD [30].
$Step4$: w and b are determined by minimizing the loss function.
$Step5$: Use test data X_{test} to test and monitor the detection accuracy of the network.

If the signal sources are coherent, the mathematical expression of receive signal is reflected in a complex constant among coherent signal sources. Assuming there are P coherent sources, it can be obtained that

$$s_p(t) = q_p s_0(t), \tag{11}$$

where $p = 1, 2, \ldots, P$ and $P \leq K$. The parameter q_p is the complex constant among coherent signal sources. The generate source $s_0(t)$ engenders P coherent signal sources incident on the array. Substituting (11) into (9), a coherent signal source model is obtained as

$$\mathbf{X_{coh}}(\mathbf{t}) = \mathbf{A}\begin{bmatrix} s_1(t) \\ s_2(t) \\ \vdots \\ s_P(t) \end{bmatrix} + \mathbf{N}(\mathbf{t}) = \mathbf{A}\begin{bmatrix} q_1 \\ q_2 \\ \vdots \\ q_P \end{bmatrix} s_0(t) + \mathbf{N}(\mathbf{t}), \tag{12}$$

$$\mathbf{X_{coh}}(\mathbf{t}) = \mathbf{A}\rho s_0(t) + \mathbf{N}(\mathbf{t}), \tag{13}$$

where ρ is a $P \times 1$ dimensional vector composed of a series of complex constants.

C. ROOT-WSF

Root-WSF is the rooting version of weighted subspace fitting (WSF) [24]. The purpose of this method is to minimize the cost function

$$f_{Root-WSF}(\theta) = Tr\left(P^{\perp}_{a(\theta)}\right)\hat{U}_S W_{Root-WSF}\hat{U}_S^H, \tag{14}$$

where

$$P^{\perp}_{a(\theta)} = I_K - a(\theta)\left(a(\theta)^H a(\theta)\right)^{-1} a(\theta)^H, \tag{15}$$

$$W_{Root-WSF} = \left(\hat{V}_S - \hat{\sigma}^2 I\right)\hat{V}_S^{-1}, \tag{16}$$

$$\hat{\sigma}^2 = \frac{1}{M-K} Tr\left(\hat{V}_n\right). \tag{17}$$

Root-WSF uses the strongest eigenvectors in a diagonal matrix ($\hat{V}_S$) and the corresponding eigenvectors in the signal subspace matrix ($\hat{U}_S$). $[\cdot]^H$ means that each element in the matrix is conjugated and transposed. $P^{\perp}_{a(\theta)}$ denotes the orthogonal projection matrix of the array steering matrix, and $W_{Root-WSF}$ is the asymptotic-optimum weight matrix. In (16), the expression I is an $M \times M$ identity matrix, and $\hat{\sigma}^2$ indicates the noise variance. In (17), T is a full rank matrix, and $\hat{V}_n$ is eigenvectors in a diagonal noise matrix. Parameter r is a key problem for the root-WSF algorithm, which indicates signal source numbers. It can be obtained by several methods [25], [26], [27] that, when $r = K$, the signals are fully non-coherent. However, it is difficult to detect the signal source number under the scenario $r < K$, where coherent signals exist. Radio frequency interference (RFI) incidents from the ground to satellites show an upward trend [28], [29]. Therefore, robust DOA estimation techniques should be considered for array signal processing in LEOP and low earth orbit (LEO) satellites. The proposed DTN will show its effectiveness in both scenarios.

D. DOA DETECTION NETWORK (DTN)

To detect the signal source number K, the DTN learns a nonlinear mapping function y_j and updates the model's weight w and bias b.

$$y_j = \sum_{i=1}^{D} w_{ji}x_i + b_j, \tag{18}$$

where $x_1, \ldots, x_D$ are input variables. The network output z_j is the result of y_j after an appropriate activation function $f(\cdot)$.

$$z_j = f\left(y_j\right), \tag{19}$$

where $j = 1, 2, \ldots J$, and J is the total output quantity.

There are several universal activation functions, such as ReLU, Sigmoid, tanh, etc. This work uses ReLU as the activation function, which is written as

$$f_{ReLU}(x) = max(0, x). \tag{20}$$

Assuming that the neural network has N layers, the overall neural network output $\mathbf{O}$ can be expressed as

$$\mathbf{O} = f(\mathbf{x}, w) = f^{(N-1)}\left(f^{(N-2)}\left(\cdots f^1(\mathbf{x})\right)\right). \tag{21}$$

$$\begin{bmatrix} x_1(t) \\ x_2(t) \\ \vdots \\ x_M(t) \end{bmatrix} = \begin{bmatrix} g_{11}e^{-j\omega_0\tau_{11}} & g_{12}e^{-j\omega_0\tau_{12}} & \cdots & g_{1K}e^{-j\omega_0\tau_{1K}} \\ g_{21}e^{-j\omega_0\tau_{21}} & g_{22}e^{-j\omega_0\tau_{22}} & \cdots & g_{2K}e^{-j\omega_0\tau_{2K}} \\ \vdots & \vdots & \ddots & \vdots \\ g_{M1}e^{-j\omega_0\tau_{M1}} & g_{M2}e^{-j\omega_0\tau_{M2}} & \cdots & g_{MK}e^{-j\omega_0\tau_{MK}} \end{bmatrix}\begin{bmatrix} S_1(t) \\ S_2(t) \\ \vdots \\ S_K(t) \end{bmatrix} + \begin{bmatrix} n_1(t) \\ n_2(t) \\ \vdots \\ n_M(t) \end{bmatrix}. \tag{7}$$

$$\begin{bmatrix} x_1(t) \\ x_2(t) \\ \vdots \\ x_M(t) \end{bmatrix} = \begin{bmatrix} e^{-j\omega_0\tau_{11}} & e^{-j\omega_0\tau_{12}} & \cdots & e^{-j\omega_0\tau_{1K}} \\ e^{-j\omega_0\tau_{21}} & e^{-j\omega_0\tau_{22}} & \cdots & e^{-j\omega_0\tau_{2K}} \\ \vdots & \vdots & \ddots & \vdots \\ e^{-j\omega_0\tau_{M1}} & e^{-j\omega_0\tau_{M2}} & \cdots & e^{-j\omega_0\tau_{MK}} \end{bmatrix}\begin{bmatrix} S_1(t) \\ S_2(t) \\ \vdots \\ S_K(t) \end{bmatrix} + \begin{bmatrix} n_1(t) \\ n_2(t) \\ \vdots \\ n_M(t) \end{bmatrix}. \tag{8}$$

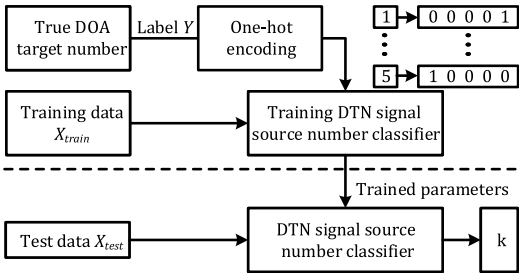

FIGURE 2. Flow chart of DOA detection network.

Then, the loss function of the neural network is given as

$$L = \sum_{i=1}^{N} \left\| k_i - \hat{k}_i \right\|^2, \tag{22}$$

where k_i is the actual number of signal sources, and $\hat{k}_i$ is the estimation number of the DTN. The stochastic gradient decent (SGD) [30] is adopted to optimize the loss function. The update process of w can be written as

$$w^t = w^{t-1} - \eta \nabla L\left(w\right), \tag{23}$$

where η is noted as the learning rate.

Table 2 summarizes the procedure of DTN. The training data X_{train} and test data X_{test} are generated by the received signal models (9) and (13) under significant condition variations. The training data X_{train} in the complex-valued domain is treated as the input of the detection network. The output layer corresponds to the number of signal sources K. The test data X_{test} is fed into the trained DTN to validate its performance. As shown in Fig. 2. the labels of DTN are the one-hot encoding of the source number, i.e., the signal source number "1" is represented by "0 0 0 0 1", "2" is represented by "0 0 0 1 0", "3" is represented by "0 0 1 0 0", etc. It solves the problem that the classifier cannot handle the coherent signals and extends the values of discrete features to Euclidean space. To a certain extent, it makes the calculation of Euclidean distance more reasonable [31].

Furthermore, the DNN has a powerful denoising capability, which can be applied to process low SNR signals [32], [33]. Comparing the second layer outputs of DTN [Figs. 3(a3) and 3(b3)] and existing methods [Figs. 4(a3) and 4(b3)], it can be seen that the denoising capability of the proposed DTN is superior to that of the existing methods in both real and imaginary part responses, as the DTN uses the received signal as input. Conversely, using the covariance matrix loses information after the networks. The computational complexity of the DTN and its comparison with AIC and MDL are explained as follows. For AIC and MDL, approximately $\mathcal{O}(M^3)$ complex multiplications are needed. This is due to that they are the methods based on the information criterion, whose computational complexity is mainly correlated to the eigen decomposition of array output covariance. For the proposed DTN method, the computational complexity is determined by the structure of the neural network. For the full connected structure, the computational complexity of DTN can be written as $\mathcal{O}(4\times(2MH+H^2+H))$, where H represents

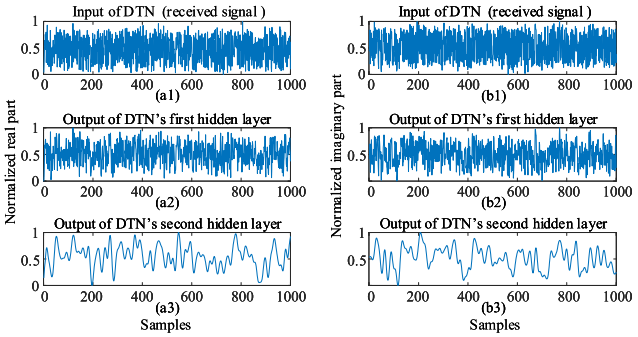

FIGURE 3. Performance of the DTN process. (a1/b1) The normalized real/imaginary part of the DTN's input (i.e., the received signal). (a2/b2) The normalized real/imaginary part of DTN's first hidden layer output. (a3/b3) The normalized real/imaginary part of DTN's second hidden layer output.

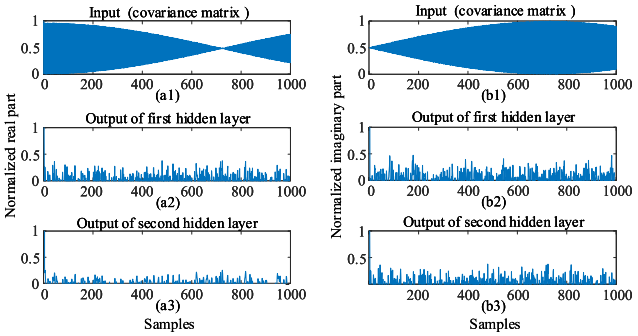

FIGURE 4. The performance of existing methods process. (a1/b1) The normalized real/imaginary part of existing methods' input (i.e., the covariance matrix). (a2/b2) The normalized real/imaginary part of existing methods' first hidden layer output. (a3/b3) The normalized real/imaginary part of existing methods' second hidden layer output.

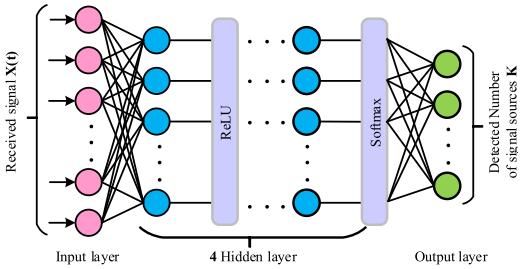

FIGURE 5. Architecture of a multiple-layered DOA detection network (DTN). Each hidden layer has 256 nodes.

the number of neurons in the hidden layer. The computational complexity of DTN is fixed after training, while the computational complexity of traditional methods will increase with the increase of the number of array elements. Therefore, for a large antenna array, the proposed DTN method will outperform the traditional signal number detection methods in terms of computational complexity.

III. SIMULATION RESULTS AND ANALYSIS

The powerful Pytorch [31] is introduced to design the DTN. All the simulations are performed in a computer with Intel Core i9 @2.3 GHz CPU and 32 GB RAM. The number of elements M in a uniform linear array (ULA) is assumed to be 10. Signal sources with different numbers $(1, 2, \ldots, 5)$ are randomly located in the angle range $[-90°, +90°]$. The

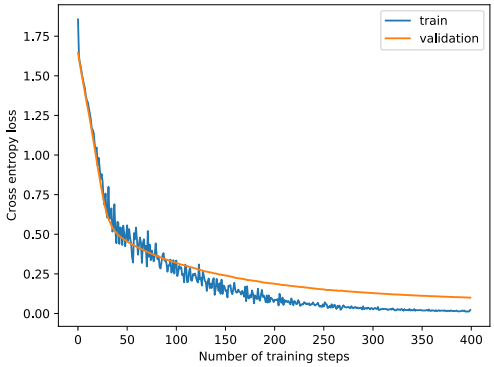

FIGURE 6. Training and validation of the DOA detection network.

inter-element spacing distance d is half-wavelength. Each received signal is a 10 by 200 matrix. The dimension of the input layer is set as 4000 after processing the received data. Under the same SNR and snapshots, 10000 samples per number of targets. A data set with 180, 000 samples is constituted, where 70% of the samples are randomly selected as the training data, and the rest 30% are used as the testing and verification data.

As shown in Fig. 5, the input of the DTN is the received signal $X(t)$. The architecture of DTN with four hidden layers is designed, and each hidden layer has 256 nodes. The ReLU activation function is used at the output of each hidden layer. The output layer is activated by the softmax function, and the output is the signal source number K. The batch size and learning rate are set to be 100 and 0.02, respectively. A well-trained DTN is obtained by updating the weights of the network. The change of cross-entropy loss with the progress of DTN training and validation is shown in Fig. 6.

A. THE DETECTION ACCURACY UNDER DIFFERENT SNAPSHOTS

The number of snapshots is an essential factor affecting the signal-source-number detection performance. Figs. 7 and 8 show the non-coherent signal source number detection accuracy in correspondence with the number of snapshots when SNR is 10 dB and −10 dB, respectively. The detection accuracy of DTN is obtained by averaging 10 tests, and the detection accuracy box plot of 10 DTN trials is depicted in Fig. 7(b). It can be seen from Fig. 7(a) that as the number of snapshots increases, the accuracy of source number detection is effectively improved. Meanwhile, the detection accuracy of AIC, MDL, CNN, and the proposed DTN becomes steady after the number of snapshots is higher than 100. Nevertheless, the AIC criterion [34] still has a relatively significant error probability in the case of a high number of snapshots. The MDL criterion [35] exhibits a superior performance under large snapshot numbers, but it performs unsatisfactorily in low snapshots scenarios compared with CNN [21] and the proposed DTN. Compared with AIC, MDL, and CNN, the proposed DTN exhibits the highest robustness of detection accuracy, even under conditions with small snapshot numbers.

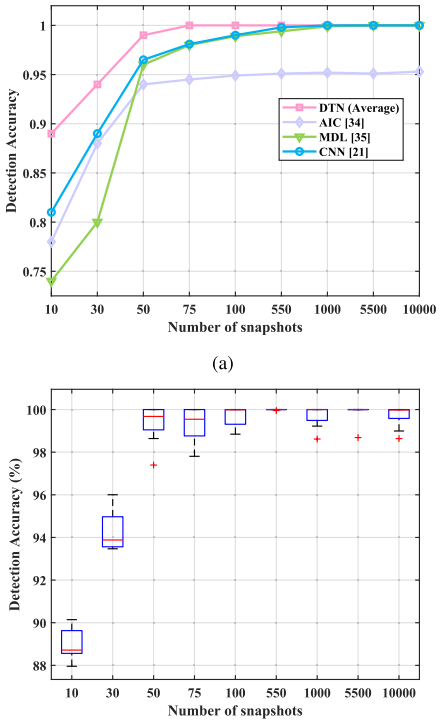

FIGURE 7. Non-coherent signal sources detection accuracy with different snapshots number (SNR = 10 dB, and 1,000 testing data are randomly selected). (a) The comparison between AIC, MDL, CNN and DTN. (b) Box plot of 10 DTN trials.

Under the condition that SNR is −10 dB, AIC [34] and MDL [35] almost fail, as shown in Fig. 8(a). Moreover, the detection accuracy of DTN is higher than CNN [21] as the label of DTN is the one-hot encoding of the source number. This extends the values of discrete features to Euclidean space, making the distance calculation more reasonable. By comparing Fig. 7(a) and Fig. 8(a), it can also be seen that the effect of snapshot number is more significant under a lower SNR value, especially for AIC, MDL, and CNN. This is because, under low SNR scenarios, the signals are buried in noises, and more snapshots are required to obtain useful characteristics. Nevertheless, as the proposed DTN considers the low SNR and low snapshots scenarios during its training process, it exhibits more robust performances under various snapshot conditions [see Fig. 7(a) and Fig. 8(a)].

B. THE DETECTION ACCURACY OF AIC, MDL, CNN, AND DTN UNDER DIFFERENT SNRs

In this subsection, the SNR varies from −20 dB to 20 dB with a 5 dB step. The detection accuracy of the proposed DTN is compared with AIC, MDL, and CNN [21] under 200 snapshots. Besides, the detection accuracy of DTN is compared with ECNet [22] under 20 snapshots and a SNR range of [0dB, 20dB], as depicted in the sub-graphs in the bottom of Fig. 9(a) and Fig. 10(a).

The detection accuracy values of non-coherent signals with different SNR are shown in Fig. 9(a), where the average detection accuracy of DTN is calculated by 10 trials. The box

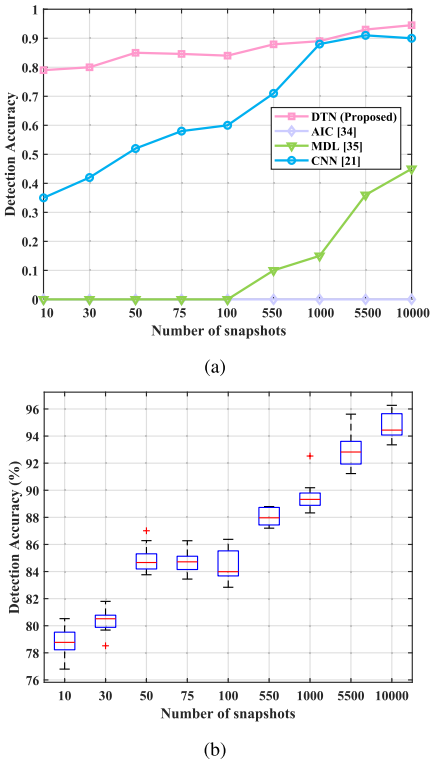

FIGURE 8. Non-coherent signal sources detection accuracy with different snapshots number (SNR = −10 dB, and 1,000 testing data are randomly selected). (a) The comparison between AIC, MDL, CNN and DTN. (b) Box plot of 10 DTN trials.

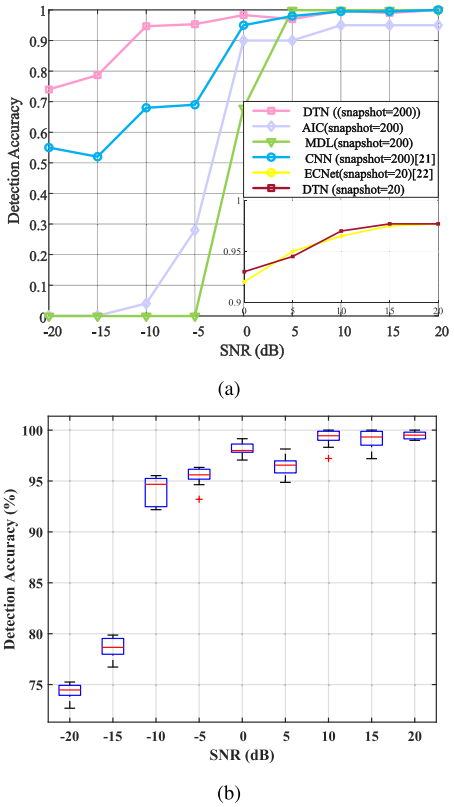

FIGURE 9. Non-coherent signals detection accuracy with different SNR (snapshots = 200 or 20, and 1,000 testing data are randomly selected). (a) The comparison between AIC, MDL, CNN, ECNet and the proposed DTN. (b) Box plot of 10 DTN trials.

plot of the 10 DTN trials is depicted in Fig. 9(b). Compared with MDL, the AIC still has a significant error probability even under high SNR values. Then, the MDL performs unsatisfactorily under low SNR conditions compared with AIC. Furthermore, the deep-learning-based DTN, CNN [21], and ECNet [22] methods outperform those conventional AIC and MDL methods in low SNR scenarios, where the application prospects of deep learning in signal source number detection can be demonstrated. As seen from the sub-graph of Fig. 9(a), DTN and ECNet [22] methods feature high detection accuracy with non-coherent signals. The low SNR (−20 dB – 0 dB) performance of ECNet is still an open issue as no relevant data is offered [22].

With coherent signal sources, the performances of AIC and MDL are not included in Fig. 10(a) since they can only detect the number of non-coherent signal sources. Besides, CNN [21] observes insufficient coherent signal detection accuracy even under high SNR scenarios (0.75 under SNR = 20 dB). Compared with the ECNet method [22], the proposed DTN is more robust for the SNR range of [0 dB, 20 dB]. The absolute coherent signal detection accuracy of DTN outperforms ECNet for the SNR range of [0 dB, 20 dB], as it is shown in the sub-graph of Fig. 10(a). Moreover, the detection accuracy of ECNet deteriorates more significantly than DTN as the SNR decreases, especially in the range of [0 dB, 10 dB].

The ECNet [22] adopts eigenvalues as the input, which is identical to AIC and MDL approaches. In contrast, the proposed DTN uses the received signals as input, where the received signals are in the complex-valued domain, and informative features are non-linearly transformed. Besides, ECNet [22] utilizes spatial smoothing to assist the network in detecting signal source numbers. The subarrays' size in [22] is 5, which is smaller than the original array's size of 10. This results in the variance of ECNet's signal source number being high than that of the proposed DTN.

C. THE DETECTION ACCURACY PERFORMANCE WITH DIFFERENT NUMBER OF SIGNAL SOURCES

The detection accuracy performance has an extraordinary significance to the application of DTN. The detection accuracy percentage is simulated when the SNR is 5dB, the number of snapshots is 200, and the number of signal sources varies from 1 to 5. The confusion matrix of DTN is depicted in Fig. 11(a), where there is no overestimation in this situation. When the number of signal sources is one, the proposed DTN can detect it with 100% accuracy. Furthermore, the average detection accuracy of both non-coherent and coherent signal sources can be up to 96.6%. The underestimation can be explained by the fact that coherent signals shall be falsely detected as one single signal. It can be seen from the box plot Fig. 11(b) that the number of correct detection will slightly decrease as the number of actual incident signals increases.

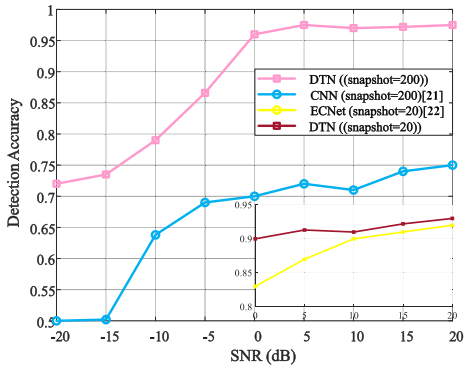

(a)

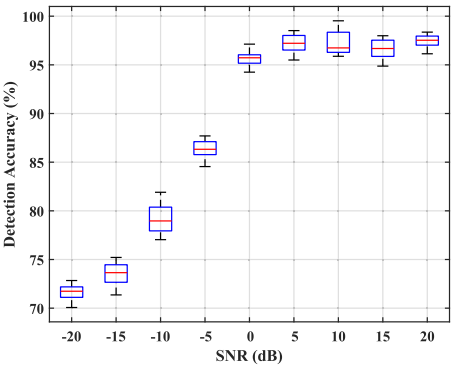

(b)

FIGURE 10. Coherent signals detection accuracy with different SNR (snapshots = 200 or 20, and 1,000 testing data are randomly selected). (a) The comparison among CNN, ECNet, and the proposed DTN. (b) Box plot of 10 DTN trials.

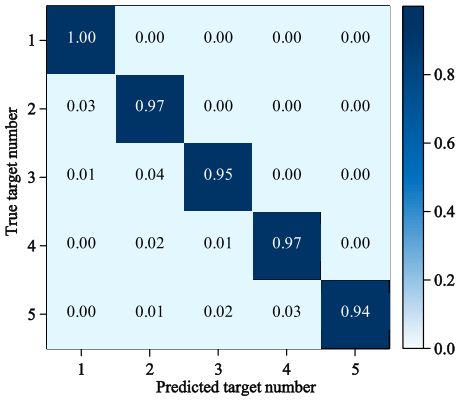

(a)

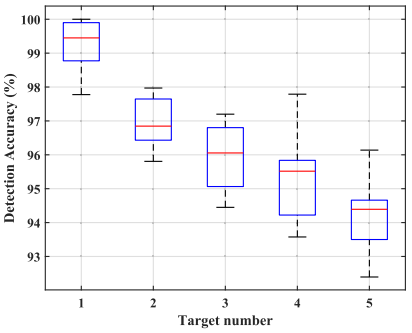

(b)

FIGURE 11. Number k of the detected signals for various actual signals number (SNR = 5dB, snapshots = 200, random non-coherent and coherent signals). (a) The confusion matrix of the detection accuracy. (b) Box plot 10 trials.

IV. DOA ESTIMATION

After the DTN, the number of signal sources can be obtained. In this section, ESPRIT, MUSIC, root-MUSIC, and root-WSF are used to estimate DOA values with the prior knowledge of signal source numbers. The root-mean-square error (RMSE) [36], [37], [38] is introduced to calculate the deviation between the estimated angles and actual angles, which can be expressed as

$$RMSE = \sqrt{\frac{1}{KR}\sum_{k=1}^{K}\sum_{r=1}^{R}\left(\hat{\theta}_{k,r} - \theta_k\right)^2}, \tag{24}$$

where K and R represent the number of targets and samples, respectively. Variable $\hat{\theta}_{k,r}$ is the k^{th} estimation angle in the r^{th} sample, and θ_k denotes the corresponding k^{th} actual angle. It means that the better accurate is accomplished as the RMSE values decrease. The angles $(\bar{\theta}_1, \bar{\theta}_2)$ are the average values after 10 estimates and RMSE are obtained with 10 Monte Carlo experiments in the follows.

A. NON-COHERENT SIGNAL ESTIMATION

The DOA estimation results of two non-coherent signals incident on a 10 - element ULA are summarized in Table 3 (SNR = 10 dB) and Table 4 (SNR = −10 dB), where two groups of signals are considered. In the first group, the first signal θ_1 arrives from −5° in azimuth, while the second signal θ_2 arrives from 5° in azimuth. In the second group, the azimuth angles are 15° and 10°, respectively.

TABLE 3. DOA estimation angles comparison under ESPRIT, MUSIC, Root-MUSIC, and Root-WSF incorporated with DTN. (SNR = 10 dB, Two signal sources detected.)

Method	$\theta_1 = -5°$ and $\theta_2 = 5°$			$\theta_1 = 15°$ and $\theta_2 = 10°$		
	$\bar{\theta}_1(°)$	$\bar{\theta}_2(°)$	RMSE	$\bar{\theta}_1(°)$	$\bar{\theta}_2(°)$	RMSE
ESPRIT	−4.9917	4.9946	0.007	14.9872	10.0139	0.0134
MUSIC	−5.0092	5.0033	0	15.0007	9.9997	0.0032
Root-MUSIC	−5.0214	4.9767	0.0224	15.0069	9.9937	0.0066
Root-WSF	**−5.0211**	**4.9765**	**0.0223**	**15.0079**	**9.9932**	**0.0074**

As shown in Table 3, all methods perform well with an azimuth angle space of 10° and 5° under the SNR of 10 dB scenario, where MUSIC has better resolution than ESPRIT, root-MUSIC, and root-WSF. Nevertheless, under the −10 dB SNR scenario, root-WSF shows even better performance (RMSE = 0.7609) than MUSIC (RMSE = 1.5811) with an azimuth angle space of 5°, as shown in Table 4.

B. COHERENT SIGNAL ESTIMATION

Under the coherent signal scenario, it is assumed that four narrow-band signals incident from −24°, −6°, 18°, and 50° under the Gaussian white noise environment. Signals −6° and 18° are the multipath reflections of the first signal source

TABLE 4. DOA estimation angles comparison under ESPRIT, MUSIC, Root-MUSIC, and Root-WSF incorporated with DTN. (SNR = −10 dB, Two signal sources detected.)

Method	$\theta_1 = -5°$ and $\theta_2 = 5°$			$\theta_1 = 15°$ and $\theta_2 = 10°$		
	$\bar{\theta}_1(°)$	$\bar{\theta}_2(°)$	RMSE	$\bar{\theta}_1(°)$	$\bar{\theta}_2(°)$	RMSE
ESPRIT	−4.5314	5.4043	0.4376	16.2229	11.1240	1.1745
MUSIC	−5.1845	5.1203	0.0945	14.1300	8.9790	1.5811
Root-MUSIC	−5.1556	5.0797	0.1236	15.2694	11.3587	0.9794
Root-WSF	**−5.0905**	**5.0669**	**0.0796**	**16.0639**	**10.1613**	**0.7609**

TABLE 5. DOA estimation angles comparison under ESPRIT, MUSIC, Root-MUSIC, and Root-WSF incorporated with DTN. (SNR = 10 dB, Four signal sources detected.)

Method	$\theta_1 = -24°, \theta_2 = -6°, \theta_3 = 18°$, and $\theta_4 = 50°$				
	$\bar{\theta}_1(°)$	$\bar{\theta}_2(°)$	$\bar{\theta}_3(°)$	$\bar{\theta}_4(°)$	RMSE
ESPRIT	−21.6952	−54.2594	−1.6404	49.9876	10.6459
MUSIC	−24.7910	−55.0023	8.6704	50.0000	10.0804
Root-MUSIC	−23.2899	−6.9984	7.9205	49.9938	2.0726
Root-WSF	**−24.0046**	**−5.9956**	**18.0119**	**49.9920**	**0.0078**

TABLE 6. DOA estimation angles comparison under ESPRIT, MUSIC, Root-MUSIC, and Root-WSF incorporated with DTN. (SNR = −10 dB, Four signal sources detected.)

Method	$\theta_1 = -24°, \theta_2 = -6°, \theta_3 = 18°$, and $\theta_4 = 50°$				
	$\bar{\theta}_1(°)$	$\bar{\theta}_2(°)$	$\bar{\theta}_3(°)$	$\bar{\theta}_4(°)$	RMSE
ESPRIT	−22.0101	−52.8369	−1.4167	49.5425	10.3579
MUSIC	−25.233	−53.7789	8.6834	50.0002	9.8107
Root-MUSIC	−23.5966	−7.0336	7.8847	49.6200	2.0786
Root-WSF	**−24.0603**	**−4.8821**	**17.9546**	**49.4248**	**0.6297**

−24°, having magnitudes equal to 1/4 and 1/2 of the first signal source, respectively. Therefore, the former three signal sources are considered coherent with each other, and the last one, 50°, is non-coherent with them.

As shown in Table 5 and Table 6, all methods with the prior knowledge of signal source numbers can successfully estimate the independent signal at 50°. However, ESPRIT and MUSIC cannot correctly estimate the coherent signals even when the actual signal numbers are given, because coherent signal sources' steering vectors are not entirely orthogonal to the noise subspace [39]. The root-WSF method features higher estimation accuracy and resolution than the root-MUSIC algorithm under SNR = 10 dB and −10 dB conditions. Therefore, root-WSF is considered to be the most accurate estimation of the DOA under the premise of knowing the number of signal sources.

The estimated angles with root-WSF based on AIC and DTN are shown in Fig. 12. It can be seen that the root-WSF based on AIC underestimates the number of signal sources, causing the root-WSF only gives two estimate angles, i.e., −24 and 50. On the other hand, the proposed DTN incorporating root-WSF successfully estimates all of the four signal sources (including three coherent signals) with a high

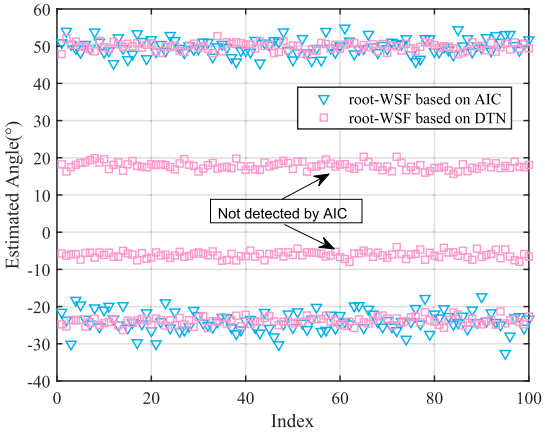

FIGURE 12. Estimated angles with root-WSF based on AIC and DTN.

resolution. Therefore, using DTN to detect the number of signal sources accurately is crucial to DOA estimation, and the proposed DTN incorporating with root-WSF will improve the DOA estimation robustness.

V. CONCLUSION

This paper proposes a DOA detection network (DTN) incorporated with root-WSF for DOA estimation. The signal source number is detected by DTN, which can effectively denoise the received signal and detect the numbers of both non-coherent and coherent signal sources with high accuracy, even under a low SNR scenario. The DTN label is a one-hot encoding of the source number, which solves the problem that the classifier cannot handle the coherent signals. It also extends the value of discrete features to Euclidean space, making the distance calculation more reasonable. The results show that the proposed DTN has superiority in detecting the signal source number with an average detection accuracy of 96.6%. Furthermore, the root-WSF is incorporated with DTN to estimate the signal sources' DOA, compensating for the defect that the spatial smoothing method needs to sacrifice the array aperture to improve the estimation accuracy and resolution. The application prospect of DTN incorporating with root-WSF is successfully demonstrated in the area of DOA estimation. Although this work is proposed targeting satellite communication scenarios, it also has the high potential to be extended to terrestrial communication systems, especially emerging systems such as 5G Beoynd and 6G networks.

REFERENCES

[1] J. Bu, K. Yu, N. Qian, X. Zuo, and J. Chang, "Performance assessment of positioning based on multi-frequency multi-GNSS observations: Signal quality, PPP and baseline solution," *IEEE Access*, vol. 9, pp. 5845–5861, 2021.

[2] B. Hao, D. An, L. Wang, Z. Li, and Y. Zhao, "A new passive localization method of the interference source for satellite communications (invited paper)," in *Proc. 9th Int. Conf. Wireless Commun. Signal Process. (WCSP)*, Oct. 2017, pp. 1–6.

[3] H. Shuai, S. Zhu, and C. Li, "Modeling and error accuracy analysis of three satellite interference source location system by low and high orbit," in *Proc. IEEE 9th Int. Conf. Electron. Inf. Emergency Commun. (ICEIEC)*, Jul. 2019, pp. 1–7.

[4] I. Ziskind and M. Wax, "Maximum likelihood localization of multiple sources by alternating projection," *IEEE Trans. Acoust., Speech Signal Process.*, vol. ASSP-36, no. 10, pp. 1553–1560, Oct. 1988.
[5] R. O. Schmidt, "Multiple emitter location and signal parameter estimation," *IEEE Trans. Antennas Propag.*, vol. AP-34, no. 3, pp. 276–280, Mar. 1986.
[6] R. Roy and T. Kailath, "Esprit-estimation of signal parameters via rotational invariance techniques," *IEEE Trans. Acoust., Speech, Signal Process.*, vol. 37, no. 7, pp. 984–995, Jul. 1989.
[7] B. Ottersten and M. Viberg, "Analysis of subspace fitting based methods for sensor array processing," in *Proc. Int. Conf. Acoust., Speech, Signal Process.*, vol. 4, Glasgow, U.K., May 1989, pp. 2807–2810.
[8] F. Gao and A. B. Gershman, "A generalized ESPRIT approach to direction-of-arrival estimation," *IEEE Signal Process. Lett.*, vol. 12, no. 3, pp. 254–257, Mar. 2005.
[9] B. D. Rao and K. V. S. Hari, "Performance analysis of root-music," *IEEE Trans. Acoust., Speech, Signal Process.*, vol. 37, no. 12, pp. 1939–1949, Dec. 1989.
[10] Y. Wang, *Theories and Algorithms of Spatial Spectrum Estimation*. Beijing, China: Tsinghua Univ. Press, 2004.
[11] E. Fishler, M. Grosmann, and H. Messer, "Detection of signals by information theoretic criteria: General asymptotic performance analysis," *IEEE Trans. Signal Process.*, vol. 50, no. 5, pp. 1027–1036, May 2002.
[12] C. Qi, Y. Wang, Y. Zhang, and Y. Han, "Spatial difference smoothing for DOA estimation of coherent signals," *IEEE Signal Process. Lett.*, vol. 12, no. 11, pp. 800–802, Nov. 2005.
[13] H. Chen, Y. Zhou, L. Tian, J. Shi, J. Hu, and M. Suzuki, "A novel modification of WSF for DOA estimation," in *Proc. IEEE Wireless Commun. Netw. Conf. (WCNC)*, Apr. 2013, pp. 2868–2873.
[14] L. Wan, R. Liu, L. Sun, H. Nie, and X. Wang, "UAV swarm based radar signal sorting via multi-source data fusion: A deep transfer learning framework," *Inf. Fusion*, vol. 78, pp. 90–101, Feb. 2022.
[15] Y. Li, Y. Huang, G. F. Pedersen, and M. Shen, "Recurrent NEAT assisted 2D-DOA estimation with reduced complexity for satellite communication systems," *IEEE Access*, vol. 10, pp. 11551–11563, 2022.
[16] L. Wan, K. Liu, and W. Zhang, "Deep learning-aided off-grid channel estimation for millimeter wave cellular systems," *IEEE Trans. Wireless Commun.*, vol. 21, no. 5, pp. 3333–3348, May 2022, doi: 10.1109/TWC.2021.3120926.
[17] W. Zhu, M. Zhang, P. Li, and C. Wu, "Two-dimensional DOA estimation via deep ensemble learning," *IEEE Access*, vol. 8, pp. 124544–124552, 2020.
[18] B. Hu, M. Liu, F. Yi, H. Song, F. Jiang, F. Gong, and N. Zhao, "DOA robust estimation of echo signals based on deep learning networks with multiple type illuminators of opportunity," *IEEE Access*, vol. 8, pp. 14809–14819, 2020.
[19] Z.-M. Liu, C. Zhang, and P. S. Yu, "Direction-of-arrival estimation based on deep neural networks with robustness to array imperfections," *IEEE Trans. Antennas Propag.*, vol. 66, no. 12, pp. 7315–7327, Dec. 2018.
[20] M. Chen, Y. Gong, and X. Mao, "Deep neural network for estimation of direction of arrival with antenna array," *IEEE Access*, vol. 8, pp. 140688–140698, 2020.
[21] W. Hu, R. Liu, X. Lin, Y. Li, X. Zhou, and X. He, "A deep learning method to estimate independent source number," in *Proc. 4th Int. Conf. Syst. Informat. (ICSAI)*, Nov. 2017, pp. 1055–1059.
[22] Y. Yang, F. Gao, C. Qian, and G. Liao, "Model-aided deep neural network for source number detection," *IEEE Signal Process. Lett.*, vol. 27, pp. 91–95, 2020.
[23] J. Zhen and X. Zhang, "Number of coherent nodes estimation based on multiple feature extraction in wireless sensor network," *IEEE Access*, vol. 8, pp. 155951–155960, 2020.
[24] A. M. Zoubir, M. Viberg, R. Chellappa, and S. Theodoridis, *Academic Press Library in Signal Processing: Array and Statistical Signal Processing*. New York, NY, USA: Academic, 2013.
[25] M. Viberg, B. Ottersten, and T. Kailath, "Detection and estimation in sensor arrays using weighted subspace fitting," *IEEE Trans. Signal Process.*, vol. 39, no. 11, pp. 2436–2449, Nov. 1991.
[26] M. Wax and I. Ziskind, "Detection of the number of coherent signals by the MDL principle," *IEEE Trans. Acoust., Speech Signal Process.*, vol. 37, no. 8, pp. 1190–1196, Aug. 1989.
[27] H. Akaike, "Information theory and an extension of the maximum likelihood principle," in *Proc. 2nd Int. Symp. Inform. Theory*, B. N. Petrov and F. Caski, Eds. 1973, pp. 267–281.
[28] S. K. Sharma, S. Chatzinotas, and B. Ottersten, "Satellite cognitive communications: Interference modeling and techniques selection," in *Proc. 6th Adv. Satell. Multimedia Syst. Conf. (ASMS) 12th Signal Process. Space Commun. Workshop (SPSC)*, Sep. 2012, pp. 111–118.
[29] H. Shuai, S. Zhu, and C. Li, "Modeling and error accuracy analysis of three satellite interference source location system by low and high orbit," in *Proc. IEEE 9th Int. Conf. Electron. Inf. Emergency Commun. (ICEIEC)*, Jul. 2019, pp. 1–7.
[30] L. Bottou, "Large-scale machine learning with stochastic gradient descent," in *Proc. COMPSTAT*, 2010, pp. 177–186.
[31] A. Paszke, S. Gross, F. Massa, A. Lerer. Bradbury, and G. Chanan, "PyTorch: An imperative style, high-performance deep learning library," in *Proc. Adv. Neural Inf. Process. Syst.* Red Hook, NY, USA: Curran Associates, 2019, pp. 8024–8035. [Online]. Available: http://papers.neurips.cc/paper/9015-pytorch-an-imperative-style-high-performance-deep-learning-library.pdf
[32] T. Wada, T. Toma, M. Dawodi, and J. Baktash, "A denoising autoencoder based wireless channel transfer function estimator for OFDM communication system," in *Proc. Int. Conf. Artif. Intell. Inf. Commun. (ICAIIC)*, Feb. 2019, pp. 530–533.
[33] M. Goutay, F. A. Aoudia, and J. Hoydis, "Deep reinforcement learning autoencoder with noisy feedback," in *Proc. Int. Symp. Modeling Optim. Mobile, Ad Hoc, Wireless Netw. (WiOPT)*, Jun. 2019, pp. 1–6.
[34] M. Wax and T. Kailath, "Detection of signals by information theoretic criteria," *IEEE Trans. Acoust., Speech, Signal Process.*, vol. ASSP-33, no. 2, pp. 387–392, Apr. 1985.
[35] J.-F. Gu and P. Wei, "Detection of the number of sources using eigenvector-based approach," in *Proc. 7th Int. Symp. Antennas, Propag. EM Theory*, Oct. 2006, pp. 1–4.
[36] H. Huang, J. Yang, H. Huang, Y. Song, and G. Gui, "Deep learning for super-resolution channel estimation and DOA estimation based massive MIMO system," *IEEE Trans. Veh. Technol.*, vol. 67, no. 9, pp. 8549–8560, Sep. 2018.
[37] M. Yang, B. Ai, R. He, C. Huang, Z. Ma, Z. Zhong, J. Wang, L. Pei, Y. Li, and J. Li, "Machine-learning-based fast angle-of-arrival recognition for vehicular communications," *IEEE Trans. Veh. Technol.*, vol. 70, no. 2, pp. 1592–1605, Feb. 2021.
[38] G. Tang, X. Gao, Z. Chen, Y. Zhang, H. Zhong, and M. Li, "Deep neural network based multiple targets DOA estimation for millimeter-wave radar," in *Proc. IEEE SmartWorld, Ubiquitous Intell. Comput., Adv. Trusted Comput., Scalable Comput. Commun., Cloud Big Data Comput., Internet People Smart City Innov. (SmartWorld/SCALCOM/UIC/ATC/CBDCom/IOP/SCI)*, Aug. 2019, pp. 433–438.
[39] R. T. Williams, S. Prasad, A. K. Mahalanabis, and L. H. Sibul, "An improved spatial smoothing technique for bearing estimation in a multipath environment," *IEEE Trans. Acoust., Speech Signal Process.*, vol. ASSP-36, no. 4, pp. 425–432, Apr. 1988.

YUNFENG LI (Student Member, IEEE) was born in Linyi, China, in 1995. She received the B.Sc. degree in electronic information science and technology from Shandong Normal University, Shandong, China, in 2017. She is currently pursuing the Ph.D. degree with the National Space Science Center (NSSC), Key Laboratory of Electronics and Information Technology for Space Systems, University of the Chinese Academy of Sciences (UCAS). She was a Visiting Ph.D. student with RF and mm-wave circuits and systems at the Department of Electronic Systems, Aalborg University, Denmark, from March 2019 to March 2020. She was a Research Assistant with RF and mm-wave circuits and systems at the Department of Electronic Systems, Aalborg University, from March 2020 to March 2021. Her main research interests include digital pre-distortion techniques, millimeter wave antenna design, and DOA signal processing. She serves as the Reviewer for IEEE Access.

YONGHUI HUANG was born in Anshan, China. He received the B.Sc. degree in electronics engineering from Tsinghua University, Beijing, China, in 1998, the M.Sc. degree in aero-spacecraft design from the University of Chinese Academy of Sciences, Beijing, in 2001, and the Ph.D. degree in wireless communication from Aalborg University, Aalborg, Denmark, in 2008.

From 2002 to 2011, he worked as a Postdoctoral Researcher and a Research Assistant at the Aalborg University. He was an Engineer at Datang Mobile of Beijing, China, from 2001 to 2002. He is currently a Professor with the National Space Science Center, Chinese Academy of Sciences, Beijing. His current research interests include deep space communication, satellite wireless communication, phased array antenna, and transmitter linearization. He is a TPC Member of IEEE CCET and IEEE WiSEE.

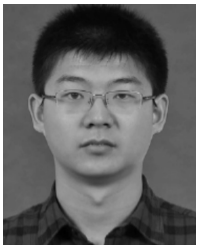

JIAN REN (Member, IEEE) was born in Dezhou, China, in 1989. He received the B.Sc. degree in electronic engineering and the M.Eng. degree in electromagnetics and microwave technology from Xidian University, Xi'an, China, in 2012 and 2014, respectively, and the Ph.D. degree from the City University of Hong Kong, Hong Kong, in 2018.

In 2015, he was a Research Assistant at the City University of Hong Kong. He is currently an Associate Professor with the National Key Laboratory of Antennas and Microwave Technology, Xidian University. His research interests include microwave circuits, metamaterials, RFID, and dielectric resonator antennas.

YING LIU received the M.S. and Ph.D. degrees from Beijing Jiaotong University, in 2003 and 2012, respectively.

She is currently a Professor with the School of Electronic and Information Engineering, Beijing Jiaotong University. Her current research interests include network architecture, network security, protocols optimization, wireless communications, and cloud computing.

GERT FRØLUND PEDERSEN (Senior Member, IEEE) was born in 1965. He received the B.Sc. and E.E. (Hons.) degrees in electrical engineering from the College of Technology in Dublin, Dublin Institute of Technology, Dublin, Ireland, in 1991, and the M.Sc.E.E. and Ph.D. degrees from Aalborg University, Aalborg, Denmark, in 1993 and 2003, respectively.

Since 1993, he has been with Aalborg University, where he is currently a Full Professor heading the Antennas, Propagation and Millimeter-wave Systems Laboratory with 25 researchers. He is also the Head of the Doctoral School on wireless communication with some 40 Ph.D. students enrolled. He has published more than 500 peer-reviewed papers, six books, 12 book chapters, and holds over 50 patents. His research interests include radio communication for mobile terminals especially small antennas, diversity systems, propagation, and biological effects. He has also worked as a Consultant for developments of more than 100 antennas for mobile terminals including the first internal antenna for mobile phones in 1994 with lowest SAR, first internal triple-band antenna in 1998 with low SAR and high TRP and TIS, and lately various multiantenna systems rated as the most efficient on the market. He has worked most of the time with joint university and industry projects and have received more than 21 M$ in direct research funding. He is currently the Project Leader of the RANGE Project with a total budget of over eight M$ investigating high performance centimetre/millimeter-wave antennas for 5G mobile phones. He has been one of the pioneers in establishing over-the-air measurement systems. The measurement technique is now well established for mobile terminals with single antennas. He was chairing the various COST groups with liaison to 3GPP and CTIA for over-the-air test of MIMO terminals. He is currently involved in MIMO OTA Measurement.

MING SHEN (Senior Member, IEEE) was born in Yuxi, China. He received the M.Sc. degree in electrical engineering from the University of Chinese Academy of Sciences (UCAS), Beijing, China, in 2005, and the Ph.D. degree in wireless communications with the Spar Nord Annual Best Thesis nomination from Aalborg University, Aalborg, Denmark, in 2010.

He has 20 years experience in RF and millimeter wave circuits and systems, including 12 years experience in CMOS RF/mixed-signal IC design. He is currently an Associate Professor in RF and mm-wave circuits and systems with the Department of Electronic Systems, Aalborg University. His current research interests include circuits and antennas for 5G and satellite communications, low power CMOS RF and millimeter wave circuits and systems, circuits and systems for biomedical imaging, and artificial intelligence. He is the grant holder and PI of three Danish national research projects and the management committee member substitute from Denmark in the EU COST Action IC1301 with the aim to gather the international efforts and address efficient wireless power transmission technologies. He is a TPC Member of IEEE NORCAS and serves as a reviewer for IEEE and Kluwer.